Earthquakes and Structures, Vol. 4, No. 2 (2013) 133-155
DOI: http://dx.doi.org/10.12989/eas.2013.4.2.133

A method for earthquake response analysis of tall flexible structure

Tielin Liu*[1,2], Yingchun Jiang[1] and Yu Luan[1]

[1]*School of Civil Engineering, Dalian University of Technology, Dalian 116024 P R China*
[2]*School of Civil Engineering, Shenyang Jianzhu University, Shenyang 110168 P R China*

(Received May 9, 2011, Revised February 12, 2012, Accepted March 12, 2012)

Abstract. The earthquake responses are studied for the tall flexible structures such as TV towers when the vertical eccentricities between the discrete nodes and the corresponding centroids of investigated lumps are considered. In practical analyses, the tall flexible structures can be made into a spatial-discrete system of some certain length of beam elements with different lengths and cross-sectional areas. These elements are used to construct the investigated lumps in this paper. The different cross-sectional areas and the different lengths of two adjacent elements lead to the appearance of vertical eccentricity between the discrete node and the centroid of investigated lump within the same investigated lump. Firstly, the governing equations are established for a typical investigated lump. Secondly, the calculating formulae of the forces and moments acting on the investigated lump are derived and provided. Finally the new dynamic equilibrium equations with modified mass matrix and assemblage of stiffness matrix have been derived for the stick MDOF model based on beam theory when the existing vertical eccentricities are considered. Numerical results demonstrate that these vertical eccentricities should be considered in order to obtain the accurate earthquake responses for the tall flexible structures.

Keywords: tall flexible structure; earthquake response; investigated lump; vertical eccentricity

1. Introduction

In the dynamic analyses of tall flexible structures such as tall TV transmission towers, tall reinforced concrete chimneys and so on, it is known that the stick MDOF (multi-degree-of-freedom) structural model on the basis of the beam theory can be used to obtain the calculating results needed for the researches and designs as well.

Many research works have been carried out about the TV towers and tall reinforced concrete chimneys. The wind-induced acceleration responses at the small observation hall of Nanjing TV tower in Nanjing, China under strong winds were found to be too high to meet the human comfort requirements. The acceleration response at the small observation hall exceeded. Some researchers have studied the wind-induced vibration responses (Reinhorn 1995, Feng 1997) and designed the control devices (Wu 2000, Cao 1998) for the Nanjing TV tower in order to reduce the acceleration response of the small observation hall to meet the human comfort requirements. Literatures (Feng

*Corresponding author, Professor, E-mail: cetlliu@sjzu.edu.cn

1998, Wu 2004) studied the finite element model updating of the Nanjing TV tower based on ambient vibration measurements for establishing an accurate and reliable dynamic model of the tower in order to design an appropriate vibration control system.

Khaloo *et al.* (2001) adopted respectively the beam element, shell element and brick solid element to investigate the linear and nonlinear response of the Milad TV tower. Halabian *et al.* (2002) analyzed the seismic response of the Milad tower. They considered not only the foundation flexibility but also the nonlinear model of the TV tower. Yahyai *et al.* (2009) developed a detailed finite element model of Milad tower and carried out the nonlinear dynamic analysis of the tower under the design earthquakes.

A 115-meter high reinforced concrete chimney collapsed on August 17, 1999 Izmit (kocaeli) earthquake in Turkey. Another similar survived chimney at the same site was calculated using the ground motions recorded at a nearby station. Literatures (Gould 2009, Akinci 2009, Huang 2007, Gould 2006, Huang 2004) studied thoroughly the collapsed chimney with different methods including the linear dynamic response spectrum, nonlinear static capacity spectrum, nonlinear dynamic analysis with shell elements, and a new 3D pushover analysis procedure. The analyzing results demonstrated that the low ductility and inadequate capacity due to a large duct were the two significant factors for the collapsed chimney.

Goyal and Maiti (1997) presented a procedure to quantify the difference between inelastic seismic resistance and elastic seismic resistance in terms of displacement ductility capacity factors for the chimney. Wilson (2003) studied the inelastic response of ten chimneys, ranging in height from 115-meter to 301-meter, subjected to earthquake excitations.

The finite element is an efficient method to solve the dynamic equilibrium equations for the tall structures in order to obtain their earthquake responses. When the stick MDOF structural model is used, the discrete beam elements are usually adopted for the tall flexible structures in practical dynamic analyses. A certain length of element is commonly used for each of the beam elements. Though very fine beam elements can be adopted theoretically, it is not often used in the practical analyses. The discrete lengths are usually different, that is to say, the spatial-discrete size is not equal. The sizes of the element's cross sections are also different because the cross-sectional areas of tall flexible structures are commonly designed to be variable. The different cross-sectional areas and the different lengths of the two adjacent elements lead to the appearance of vertical eccentricity between the discrete node and the corresponding centroid of the investigated lump (see point i and point C in the schematic Figs. 1 and 2 where the shade parts are the

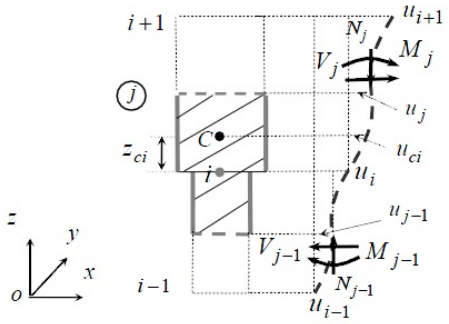

Fig. 1 Investigated lump i and its deformation for the $z_{ci} \geq 0$ case

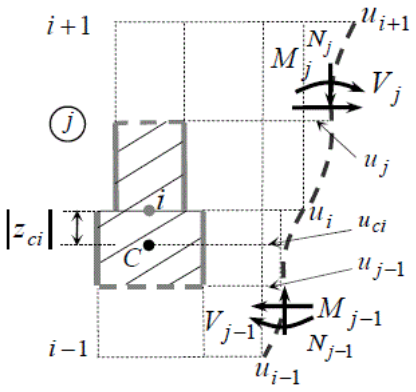

Fig. 2 Investigated lump i and its deformation for the $z_{ci} < 0$ case

investigated lumps). When we think the conventional dynamic equilibrium equations over, we can find that the conventional governing equations are not quite exact. As a matter of fact, the conventional dynamic equilibrium equations based on the stick MDOF models imply that the vertical eccentricities between the discrete nodes and the corresponding centroids of investigated lumps are omitted. The translation equations should be established about the centroid of investigated lump but not about the discrete node based on Newton's second law of motion. The rotational equation for each investigated lump should also pivot about the horizontal axis through its centroid but should not hold about the horizontal axis through the discrete node within the same investigated lump. The distance between the discrete node and the centroid within the same investigated lump is called vertical eccentricity in this paper. In the stick MDOF model, the lumped mass is commonly used by the researchers. Namely, only the inertial forces are considered in the calculation. It means that the rotary inertias about the horizontal axis are usually neglected for the earthquake responses when the tall TV towers and tall chimneys subjected to the earthquake loads.

Though there have been many research literatures about tall flexible structures such as TV towers and tall chimneys based on beam models, to the best of our knowledge, the vertical eccentricities mentioned above were not considered up to now in the dynamic analyses for real tall flexible structures.

In this paper, the concept of investigated lump is presented for the tall flexible structures based on stick MDOF model. The modified dynamic equilibrium equations are presented. A new mass matrix, which can exactly describe the effect of vertical eccentricities between the discrete nodes and the corresponding centroids of investigated lumps, is proposed to modify the conventional mass matrix that is now widely used in the dynamic equilibrium equations. The conventional assemblage of stiffness matrix is also modified because of the existing vertical eccentricities. Not only the inertial forces of the investigated lumps are considered but also the rotary inertias of the investigated lumps are also taken into account. The earthquake responses of Nanjing TV transmission tower are studied finally.

2. Governing equations of the investigated lumps

It is known that the cross section is variable in most tall flexible structures. When such a structure is made into a spatial-discrete system, we obtain some elements of different lengths and different cross-sectional areas along the axial direction of the structure in order to get the stick MDOF analysis model. These elements are used to construct the investigated lumps that will be used as the investigated objects in this paper. An investigated lump consists of half the upper element and half the lower element around the discrete node that is inside the investigated lump. It can be easily found that the centroid of the investigated lump is generally not at the same point of the corresponding discrete node (see Figs.1 and 2). The differences of the cross-sectional areas and the lengths of the discrete elements cause that the centroid of the investigated lump and the corresponding discrete node inside the same investigated lump are not at the same point.

The term eccentricity is used here to describe the distance between the discrete node and the centroid of the investigated lump within one investigated lump. Fig. 1 shows a typical investigated lump i (Nodal numbering i is also used to denote the i-th investigated lump in this paper) for the eccentricity $z_{ci} \geq 0$ case. For example, if there is an observation hall on the TV tower, the case of investigated lump in Fig. 1 arises. That is because the cross-sectional area of the observation hall is bigger than that of its lower part of the structure. Fig. 2 is for the eccentricity $z_{ci} < 0$ case. This case exists widely because the cross-sectional area changes small gradually in the upward direction for most parts of the tall flexible structure. Let the eccentricity to be a positive quantity if the discrete node is under the centroid C (see Fig. 1) and the eccentricity to be a negative quantity if the discrete node is over the centroid C (see Fig. 2) in the same investigated lump.

In Figs. 1 and 2 N_j, V_j and M_j are respectively the median axial force, median shear force and median bending moment acting on the median cross section of element j. N_{j-1}, V_{j-1} and M_{j-1} the ones of element $j-1$. In fact they are also the forces and the bending moments acting on the investigated lump i. h_j and h_{j-1} are respectively the lengths of elements j and $j-1$. u_j and u_{j-1} are the transverse displacements at the center of elements j and $j-1$ respectively. u_{ci} is the transverse displacement of centroid C of the investigated lump i. u_i is the transverse displacement of node i, u_{i+1} the node $i+1$ and u_{i-1} the node $i-1$.

Using the function of deflection curve of the beam, we can obtain explicitly the following formulae

$$u_j = \left(\frac{u_i + u_{i+1}}{2} + \frac{\theta_i - \theta_{i+1}}{8} h_j\right) \tag{1a}$$

$$u_{j-1} = \left(\frac{u_{i-1} + u_i}{2} + \frac{\theta_{i-1} - \theta_i}{8} h_{j-1}\right) \tag{1b}$$

For the case of $z_{ci} \geq 0$,

$$u_{ci} = a_i(u_i - u_{i+1}) + u_i + z_{ci}\theta_i - \frac{z_{ci}^2}{2h_j}(\theta_i - \theta_{i+1}) + b_i(\theta_i + \theta_{i+1}) \tag{2a}$$

where $a_i = \left(\frac{2z_{ci}^3}{h_j^3} - \frac{3z_{ci}^2}{h_j^2} - \frac{\eta_j z_{ci}}{h_j}\right)\frac{1}{1+\eta_j}$, $b_i = \left(\frac{z_{ci}^3}{h_j^2} - \frac{3z_{ci}^2}{2h_j} - \frac{\eta_j z_{ci}}{2}\right)\frac{1}{1+\eta_j}$. $\eta_j = \frac{12(EI)_j}{(GA_s)_j h_j^2}$ is the

modified coefficient when considering the shear deformation in transverse direction.

For the case of $z_{ci} < 0$,

$$u_{ci} = [a_i^{/}(u_{i-1} - u_i) + u_{i-1} + (h_{j-1} + z_{ci})\theta_{i-1} - \frac{(h_{j-1} + z_{ci})^2}{2h_{j-1}}(\theta_{i-1} - \theta_i) + b_i^{/}(\theta_{i-1} + \theta_i) \tag{2b}$$

where

$$a_i^{/} = [\frac{2(h_{j-1} + z_{ci})^3}{h_{j-1}^3} - \frac{3(h_{j-1} + z_{ci})^2}{h_{j-1}^2} - \frac{\eta_{j-1}(h_{j-1} + z_{ci})}{h_{j-1}}]\frac{1}{1+\eta_{j-1}}$$

$$b_i^{/} = [\frac{(h_{j-1} + z_{ci})^3}{h_{j-1}^2} - \frac{3(h_{j-1} + z_{ci})^2}{2h_{j-1}} - \frac{\eta_{j-1}(h_{j-1} + z_{ci})}{2}]\frac{1}{1+\eta_{j-1}}.$$

The vertical and transverse governing equations for the investigated lump i are respectively

$$m_i \ddot{w}_{ci} = N_{j-1} - N_j - m_i g \tag{3}$$

$$m_i \ddot{u}_{ci} = V_j - V_{j-1} \tag{4}$$

where m_i is the mass, $\ddot{w}_{ci}$ and $\ddot{u}_{ci}$ respectively the vertical and horizontal accelerations of the centriond C of the investigated lump i.

The rotational equation about the horizontal axis (y-axis) through the centroid of the investigated lump i can be obtained as

$$J_{ci}\ddot{\theta}_i = (M_j - M_{j-1}) + V_j(\frac{h_j}{2} - z_{ci}) + V_{j-1}(\frac{h_{j-1}}{2} + z_{ci}) + N_j(u_j - u_{ci}) + N_{j-1}(u_{ci} - u_{j-1}) \tag{5}$$

where J_{ci} is the moment of inertia of investigated lump i about the y-axis through its centroid C, $\ddot{\theta}_i$ the rotational acceleration of the investigated lump. The last two terms on the right-hand side of Eq. (5) show the "extra moments" caused by the vertical dead loads and the axial forces coming from vertical deformations.

It should be pointed that the Eq. (5) holds for the both cases of $z_{ci} \geq 0$ and $z_{ci} < 0$. The $z_{ci} \geq 0$ case does not exit for the top investigated lump and the $z_{ci} < 0$ case does not exit for the bottom investigated lump.

From Fig. 3, it can be seen that the following equation holds not only for $z_{ci} \geq 0$ case but also for the $z_{ci} < 0$ case noticing that the eccentricity z_{ci} itself is negative in Fig. 2.

$$\ddot{u}_i = \ddot{u}_{ci} - z_{ci}\ddot{\theta}_i \tag{6}$$

3. Median forces and median bending moment of the element

Fig. 4 shows a typical beam element j between two discrete nodes i and $i+1$ of the tall

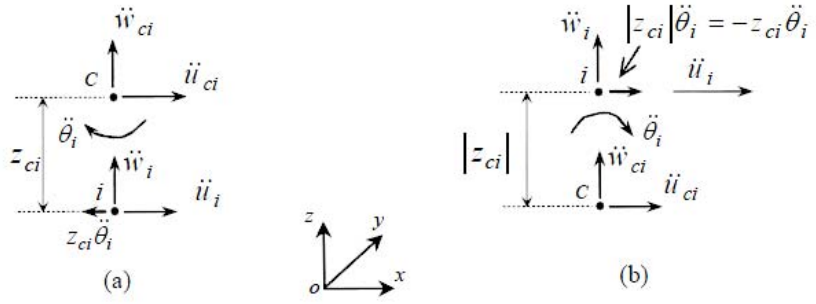

Fig. 3 Acceleration relations between node i and the corresponding centroid C of the investigated lump: (a) for the $z_{ci} \geq 0$ case and (b) for the $z_{ci} < 0$ case

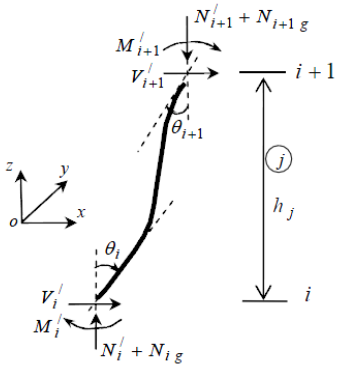

Fig. 4 Deformations, axial forces, shear forces and bending moments at both ends of segment j

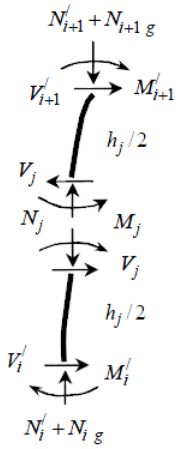

Fig. 5 Free-body diagrams of the upper and lower part of segment j by making an artificial cut through its median cross section

flexible structure. The corresponding axial forces, shear forces and bending moments at the both ends of the element j are shown in Fig. 4. The positive shear forces, bending moments, displacements and angles of rotation are in the directions of the coordinate axes. The positive axial force corresponds to the compressive force. Following the beam theory with the shear deformation and the axial force considered, the axial forces, shear forces and bending moments at the both ends of the element j can be written as follows

$$N_{i+1}^{/} = N_i^{/} = \frac{(EA)_j}{h_j}(w_i - w_{i+1}) \tag{7}$$

$$V_{i+1}^{/} = -V_i^{/} = K_{1j}(u_{i+1} - u_i) + K_{2j}(\theta_i + \theta_{i+1}) \tag{8}$$

$$M_i^{/} = K_{2j}(u_{i+1} - u_i) + K_{3j}\theta_i + K_{4j}\theta_{i+1} \tag{9}$$

$$M_{i+1}^{/} = K_{2j}(u_{i+1} - u_i) + K_{4j}\theta_i + K_{3j}\theta_{i+1} \tag{10}$$

where $K_{1j} = \frac{12(EI)_j}{h_j^3}\frac{1}{1+\eta_j} - \frac{6N_j}{5h_j}$, $K_{2j} = -\frac{6(EI)_j}{h_j^2}\frac{1}{1+\eta_j} + \frac{N_j}{10}$, $K_{3j} = \frac{4(EI)_j}{h_j}\frac{1+0.25\eta_j}{1+\eta_j} - \frac{2N_j h_j}{15}$, $K_{4j} = \frac{2(EI)_j}{h_j}\frac{1-0.5\eta_j}{1+\eta_j} + \frac{N_j h_j}{30}$. Subscript j denotes the j-th element (see Fig. 4). $N_i^{/}$ and $N_{i+1}^{/}$ are respectively the axial compressive forces of the bottom end and top end of element j coming from its vertical deformation, $V_i^{/}$ and $V_{i+1}^{/}$ the shear forces, $M_i^{/}$ and $M_{i+1}^{/}$ the bending moments. $(EI)_j$, $(GA)_j$ and $(EA)_j$ are respectively the bending stiffness, shear stiffness and axial stiffness of element j. $N_j = N_{ig} + N_i^{/}$ is the axial force acting on element j. N_{ig} is the axial force coming from the dead load of the structure above node i and N_{i+1g} the dead load above node $i+1$. w_i and θ_i are respectively the vertical displacement and rotational angle of node i. w_{i+1} and θ_{i+1} are respectively the vertical displacement and rotational angle of node $i+1$.

Eliminate u_i and u_{i+1} by subtracting Eq. (10) from Eq. (9), we have

$$M_i^{/} - M_{i+1}^{/} = [2(EI)_j / h_j - N_j h_j / 6](\theta_i - \theta_{i+1}). \tag{11}$$

Fig. 5 shows the free-body diagrams of upper half part and lower half part of the element j by an artificial cut at the median cross section of element j. We can derive the formulae of median axial force, median shear force and median bending moment for element j from the free-body diagrams.

Considering the equilibrium of the upper half part of element j, we have

$$M_{i+1}^{/} = M_j - V_j h_j / 2 - N_j(u_{i+1} - u_j) \tag{12}$$

Considering the equilibrium of the lower half part of element j, we have

$$M_i^I = -M_j - V_j h_j/2 - N_j(u_j - u_i) \tag{13}$$

and

$$V_j = K_{1j}(u_{i+1} - u_i) + K_{2j}(\theta_i + \theta_{i+1}) \tag{14}$$

Eliminate u_j by using Eq. (1a) and then substitute Eqs. (12) and (13) into Eq. (11), the median bending moment of element j is obtained as follows

$$M_j = K_{5j}(\theta_{i+1} - \theta_i) \tag{15}$$

where $K_{5j} = (EI)_j/h_j + N_j h_j/24$.

4. Modified dynamic equilibrium equations for the stick MDOF model

In Section 2 the governing equations about the centroid of a typical investigated lump i have been established and the forces and the bending moment acting on the investigated lump i were provided in Section 3. We will use them to derive the dynamic equilibrium equations about the discrete nodes for the spatial-discrete system of tall flexible structures based on the stick MDOF model.

4.1 Dynamic equilibrium equations of the investigated lumps about the centroids

Substitute Eq. (14) into Eq. (4), we obtain transverse equation of equilibrium for i-th investigated lump as follows

$$m_i \ddot{u}_{ci} - K_{1j-1}u_{i-1} + (K_{1j} + K_{1j-1})u_i - K_{1j}u_{i+1} + K_{2j-1}\theta_{i-1} + (K_{2j-1} - K_{2j})\theta_i - K_{2j}\theta_{i+1} = 0. \tag{16}$$

After substituting Eqs. (7), (14), (15) and $N_j = N_{ig} + N_i^I$ into Eq. (5) and rewriting Eqs. (16), and (5) in the matrix form, we can obtain the following governing equations for the investigated lumps subject to the horizontal earthquake load

$$\begin{bmatrix} M & 0 \\ 0 & J_c \end{bmatrix}\begin{Bmatrix} \ddot{U}_c \\ \ddot{\Theta} \end{Bmatrix} + \begin{bmatrix} K_u & K_{u\theta} \\ K_{\theta u} & K_\theta \end{bmatrix}\begin{Bmatrix} U \\ \Theta \end{Bmatrix} + \begin{bmatrix} 0 & 0 \\ K_{\theta u}^I & K_\theta^I \end{bmatrix}\begin{Bmatrix} U \\ \Theta \end{Bmatrix} + \begin{bmatrix} 0 & 0 \\ K_{\theta u}^I & K_\theta^I \end{bmatrix}\begin{Bmatrix} U \\ \Theta \end{Bmatrix} = -\begin{bmatrix} M & 0 \\ 0 & 0 \end{bmatrix}\ddot{u}_g \begin{Bmatrix} E_1 \\ E_1 \end{Bmatrix} \tag{17}$$

where $\ddot{U}_c = [\ddot{u}_{c1} \ \ddot{u}_{c2} \ \cdots \ \ddot{u}_{cn}]^T$, $\ddot{\Theta} = [\ddot{\theta}_1 \ \ddot{\theta}_2 \ \cdots \ \ddot{\theta}_n]^T$, $M = diag[m_1 \ m_2 \ \cdots \ m_n]$, $J_c = diag[J_{c1} \ J_{c2} \ \cdots \ J_{cn}]$. $E_1 = [1 \ 1 \ \cdots \ 1]^T_{n\times 1}$ is unit vector. U is the vector that consists of the nodal transverse displacements relative to the foundation. Θ is the vector composed of the rotational angles of the investigated lumps. $\ddot{u}_g$ is the horizontal acceleration history of the foundation. Matrices K_u, $K_{u\theta}$, $K_{\theta u}$, K_θ, K_θ^I, $K_{\theta u}^I$, $K_{\theta u}^I$ and K_θ^I are shown in Appendix A. In fact, the four partitioned matrices K_u, $K_{u\theta}$, $K_{\theta u}$ and K_θ in Eq. (17) are just the same assembled stiffness matrices that are used in the conventional governing equations for the stick MDOF structural

model. Matrices $K_{\theta u}^{I}$ and K_{θ}^{I} arise from the vertical eccentricities. The matrix $K_{\theta u}^{I}$ has the same form for the two cases of $z_{ci} \geq 0$ and $z_{ci} < 0$, and K_{θ}^{I} has the same characteristics as $K_{\theta u}^{I}$. Matrices $K_{\theta u}^{/}$ and $K_{\theta}^{/}$ arise also because of the vertical eccentricities. But they are needed to consider the two different cases ($z_{ci} \geq 0$ or $z_{ci} < 0$) of the investigated lumps in order to correctly assemble the matrices $K_{\theta u}^{/}$ and $K_{\theta}^{/}$.

Multiplying Eq. (16) by z_{ci}, we can obtain the following relations in matrix form

$$\begin{bmatrix} 0 & 0 \\ K_{\theta u}^{I} & K_{\theta}^{I} \end{bmatrix} \begin{Bmatrix} U \\ \Theta \end{Bmatrix} = \begin{bmatrix} 0 & 0 \\ M_z & 0 \end{bmatrix} \begin{Bmatrix} \ddot{U}_c \\ \ddot{\Theta} \end{Bmatrix} \tag{18}$$

where $M_z = diag\left[m_1 z_{c1} \quad m_2 z_{c2} \quad \cdots \quad m_n z_{cn}\right]$.

Substituting Eq. (18) into Eq. (17), we have another type of governing equations for the investigated lumps under horizontal earthquake load as follows

$$\begin{bmatrix} M & 0 \\ M_z & J_c \end{bmatrix} \begin{Bmatrix} \ddot{U}_c \\ \ddot{\Theta} \end{Bmatrix} + \begin{bmatrix} K_u & K_{u\theta} \\ K_{\theta u} & K_{\theta} \end{bmatrix} \begin{Bmatrix} U \\ \Theta \end{Bmatrix} + \begin{bmatrix} 0 & 0 \\ K_{\theta u}^{/} & K_{\theta}^{/} \end{bmatrix} \begin{Bmatrix} U \\ \Theta \end{Bmatrix} = -\begin{bmatrix} M & 0 \\ 0 & 0 \end{bmatrix} \ddot{u}_g \begin{Bmatrix} E_1 \\ E_1 \end{Bmatrix}. \tag{19}$$

4.2 Dynamic equilibrium equations of the investigated lumps about the discrete nodes

Let $Z_c = diag\left[z_{c1} \quad z_{c2} \quad \cdots \quad z_{cn}\right]$, then $M_z = MZ_c$. Multiplying matrix M by the matrix form of Eq. (6), we have

$$M\ddot{U}_c = M\ddot{U} + M_z\ddot{\Theta} \tag{20}$$

Noticing $J = J_c + MZ_c^2$, we have

$$MZ_c\ddot{U}_c + J_c\ddot{\Theta} = MZ_c(\ddot{U} + Z_c\ddot{\Theta}) + (J - MZ_c^2)\ddot{\Theta}. \tag{21}$$

That is

$$M_z\ddot{U}_c + J_c\ddot{\Theta} = M_z\ddot{U} + J\ddot{\Theta} \tag{22}$$

where $J = diag\left[J_1 \quad J_2 \quad \cdots \quad J_n\right]$, J_i is the moment of inertia of investigated lump i about the horizontal axis(y -axis) through the discrete node inside the i -th investigated lump.

Rewrite Eq. (20) and Eq. (22) in the following matrix form as

$$\begin{bmatrix} M & 0 \\ M_z & J_c \end{bmatrix} \begin{Bmatrix} \ddot{U}_c \\ \ddot{\Theta} \end{Bmatrix} = \begin{bmatrix} M & M_z \\ M_z & J \end{bmatrix} \begin{Bmatrix} \ddot{U} \\ \ddot{\Theta} \end{Bmatrix} \tag{23}$$

Finally, the modified governing equations about the spatial-discrete nodes for the dynamic analysis of tall stick MDOF model is obtained

$$\begin{bmatrix} M & M_z \\ M_z & J \end{bmatrix}\begin{Bmatrix} \ddot{U} \\ \ddot{\Theta} \end{Bmatrix}+\begin{bmatrix} K_u & K_{u\theta} \\ K_{\theta u}+K'_{\theta u} & K_\theta+K'_\theta \end{bmatrix}\begin{Bmatrix} U \\ \Theta \end{Bmatrix}=-\begin{bmatrix} M & 0 \\ 0 & 0 \end{bmatrix}\ddot{u}_g\begin{Bmatrix} E_1 \\ E_1 \end{Bmatrix} \tag{24}$$

As is well know, the conventional dynamic equations for the stick MDOF model is

$$\begin{bmatrix} M & 0 \\ 0 & J \end{bmatrix}\begin{Bmatrix} \ddot{U} \\ \ddot{\Theta} \end{Bmatrix}+\begin{bmatrix} K_u & K_{u\theta} \\ K_{\theta u} & K_\theta \end{bmatrix}\begin{Bmatrix} U \\ \Theta \end{Bmatrix}=-\begin{bmatrix} M & 0 \\ 0 & 0 \end{bmatrix}\ddot{u}_g\begin{Bmatrix} E_1 \\ E_1 \end{Bmatrix}. \tag{25}$$

Comparing Eq. (25) with Eq. (24), it can be seen that the conventional global mass matrix and global stiffness matrix, that are widely used up to now, should be modified for the reasons of vertical eccentricities in order to calculate the dynamic response of tall structure accurately. Eq. (24) instead of Eq. (25) should be used as the governing equations for the problems of earthquake response based on the tall stick MDOF structural model.

Eq. (24) reduces Eq. (25) if the phenomena of vertical eccentricities disappeared.

It should be pointed that Eq. (24) can be used in the other problems of dynamic response of tall flexible structure based on stick MDOF model if the right-hand side earthquake load is changed into a specified dynamic load, e.g. the impact loading. The non-linear dynamic analysis of tall flexible structure can be carried out by using the incremental form of modified governing Eq. (24) if the hysteretic behaviors are known on the basis of experimental results.

It is not difficult to obtain the governing equations in matrix form when the vertical and horizontal earthquake loads are considered together. The matrix form is

$$\begin{bmatrix} M & 0 & 0 \\ 0 & M & M_z \\ 0 & M_z & J \end{bmatrix}\begin{Bmatrix} \ddot{W} \\ \ddot{U} \\ \ddot{\Theta} \end{Bmatrix}+\begin{bmatrix} K_w & 0 & 0 \\ 0 & K_u & K_{u\theta} \\ 0 & K_{\theta u}+K'_{\theta u} & K_\theta+K'_\theta \end{bmatrix}\begin{Bmatrix} W \\ U \\ \Theta \end{Bmatrix}=-\begin{bmatrix} M & 0 & 0 \\ 0 & M & 0 \\ 0 & 0 & 0 \end{bmatrix}\begin{Bmatrix} \ddot{w}_g E_1 \\ \ddot{u}_g E_1 \\ E_1 \end{Bmatrix} \tag{26}$$

where $\ddot{w}_g$ is the vertical acceleration history of the foundation. K_w is the assemblage of axial element stiffness matrix. $\ddot{W}$ is the vector consist of the nodal vertical accelerations relative to the foundation. W is the vector consist of the nodal vertical displacements relative to the foundation. It should be pointed that M_z, $K'_{\theta u}$, and K'_θ vanish when eccentricity $z_{ci}=0$ and then Eq. (26) reduces the conventional dynamic equations.

4.3 Dynamic equilibrium equations with rotary inertia vanished

When the beam elements are adopted to study the real tall flexible structure, the longitudinal size of the discrete element in practical application is usually not much smaller than its lateral size. The two types of sizes may approximately be equal or even the longitudinal size is longer than the lateral size of the element. That is to say, the moment of inertia of investigated lump may be a big quantity. But the angular accelerations are commonly small quantities. When the angular accelerations are so small that the rotary inertias of the investigated lumps are neglected, Eq. (26) can be changed into the following forms according to the partitioned matrices

$$M\ddot{W}+K_w W=-M\ddot{w}_g E_1 \tag{27}$$

$$M\ddot{U}+K_u U+K_{u\theta}\Theta=-M\ddot{u}_g E_1 \tag{28}$$

$$M_z\ddot{U} + (K_{\theta u} + K'_{\theta u})U + (K_\theta + K'_\theta)\Theta = 0 \tag{29}$$

From Eq. (29), we obtain

$$\Theta = -(K_\theta + K'_\theta)^{-1}(K_{\theta u} + K'_{\theta u})U - (K_\theta + K'_\theta)^{-1}M_z\ddot{U} \tag{30}$$

Substituting Eq. (30) into Eq. (28) to eliminate Θ, we have

$$\begin{aligned}&[M - K_{u\theta}K_\theta^{-1}M_z - K_{u\theta}K_\theta'^{-1}M_z]\ddot{U}\\&+[K_u - K_{u\theta}K_\theta^{-1}K_{\theta u} - K_{u\theta}K_\theta^{-1}K'_{\theta u} - K_{u\theta}K_\theta'^{-1}K_{\theta u} - K_{u\theta}K_\theta'^{-1}K'_{\theta u}]U = -M\ddot{u}_g E_1\end{aligned} . \tag{31}$$

For the conventional dynamic Eq. (25), it is known that the equation with the rotary inertia omitted is

$$M\ddot{U} + (K_u - K_{u\theta}K_\theta^{-1}K_{\theta u})U = -M\ddot{u}_g E_1 . \tag{32}$$

Comparing Eq. (31) with Eq. (32), it can be found that $-K_{u\theta}K_\theta^{-1}M_z - K_{u\theta}K_\theta'^{-1}M_z$ is the additional term of the mass matrix and $-K_{u\theta}K_\theta^{-1}K'_{\theta u} - K_{u\theta}K_\theta'^{-1}K_{\theta u} - K_{u\theta}K_\theta'^{-1}K'_{\theta u}$ the additional term of stiffness matrix because of the vertical eccentricities. Eq. (31) instead of Eq. (32) should be used as the governing equations for the earthquake response of tall stick MDOF model with the rotary inertia neglected.

Eq. (31) reduces Eq. (32) if the phenomena of eccentricities disappeared.

Finally the matrix form of the governing equations neglecting the rotary inertia can be written as follows

$$\begin{aligned}&\begin{bmatrix} M & 0 \\ 0 & M - K_{u\theta}K_\theta^{-1}M_z - K_{u\theta}K_\theta'^{-1}M_z \end{bmatrix}\begin{Bmatrix}\ddot{W}\\ \ddot{U}\end{Bmatrix} + \begin{bmatrix} K_w & 0 \\ 0 & K_u - K_{u\theta}K_\theta^{-1}K_{\theta u}\end{bmatrix}\begin{Bmatrix}W\\U\end{Bmatrix}\\&+\begin{bmatrix}0 & 0\\ 0 & -K_{u\theta}K_\theta^{-1}K'_{\theta u} - K_{u\theta}K_\theta'^{-1}K_{\theta u} - K_{u\theta}K_\theta'^{-1}K'_{\theta u}\end{bmatrix}\begin{Bmatrix}W\\U\end{Bmatrix} = -\begin{bmatrix}M & 0\\ 0 & M\end{bmatrix}\begin{Bmatrix}\ddot{w}_g E_1\\ \ddot{u}_g E_1\end{Bmatrix}\end{aligned} \tag{33}$$

5. Earthquake responses of tall flexible structures

5.1 Test of the new method

To test the correctness of the present method, the ratios of c/c_0 are plotted against a/Λ to compare with those of the exact theory (Kolsky 1953), where c is the phase velocity that was calculated by using the method presented in this paper, $c_0 = \sqrt{E/\rho}$, a the radius of the bar with constant cross section throughout its length and Λ the wavelength of the flexural waves.

It can be seen from Fig. 6 that curve given by the present method agrees very well with that of the exact theory. It can be concluded that the method presented in this paper is valid and accurate to study the flexural waves.

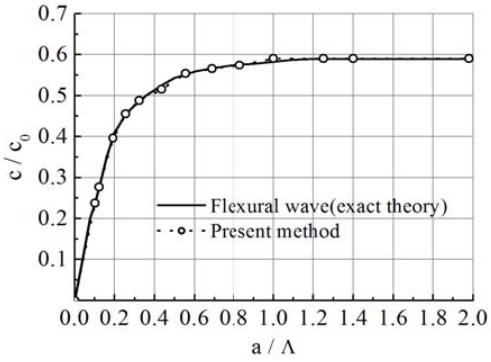

Fig. 6 Phase velocity of flexural waves in cylindrical bars (for $\nu = 0.29$)

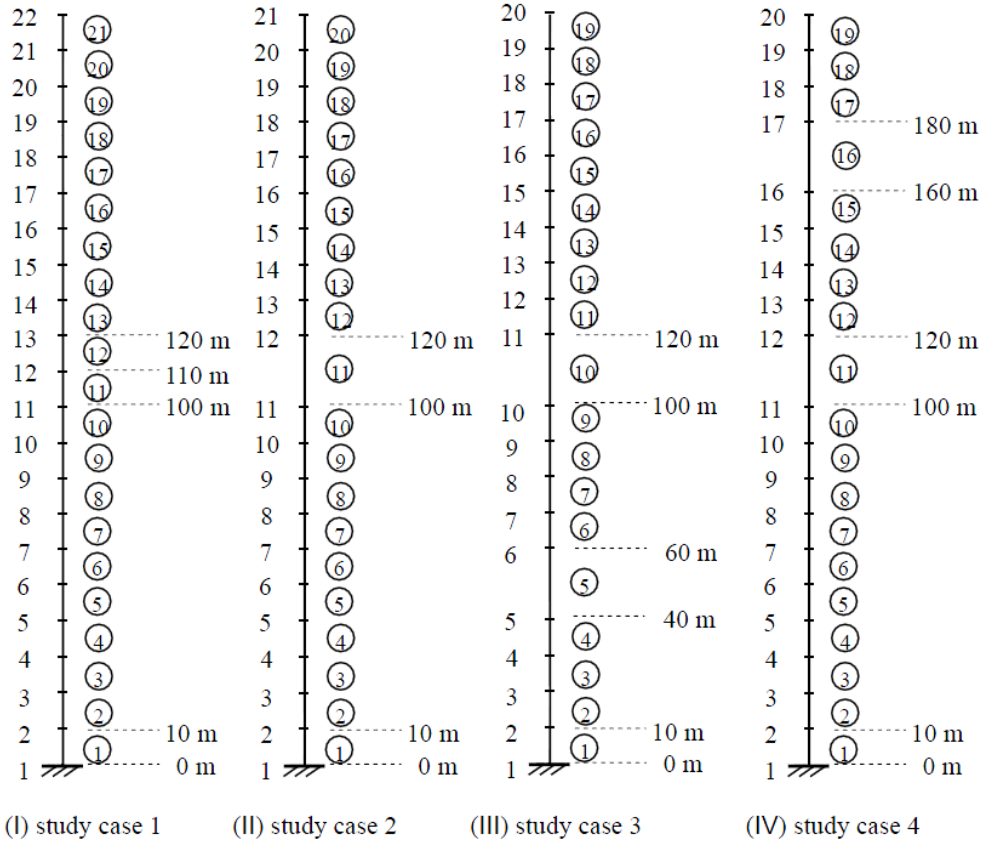

Fig. 7 Sketch of the discrete models of an ideal 210 m chimney with equal cross section area

5.2 Earthquake acceleration records used

Four earthquake acceleration records (see Table 1) on four different soil types selected from the

Table 1 Seismic waves used

Soil site	Earthquake	Date	Direction	Station and component	PGA /g
Rock	Kocaeli, Turkey	1999/08/17	Horizontal	KOCAELI/GBZ000	0.244
			Vertical	KOCAELI/GBZ-UP	0.203
Soft rock	Morgan Hill	1984/04/24	Horizontal	MORGAN/G06000	0.222
			Vertical	MORGAN/G06-UP	0.405
Stiff soil	Chichi, Taiwan	1999/09/20	Horizontal	CHICHI/CHY006-N	0.345
			Vertical	CHICHI/CHY006-V	0.202
Soft soil	Imperial Valley	1979/10/15	Horizontal	IMPVALL/H-E03140	0.266
			Vertical	IMPVALL/H-E03-UP	0.127

PEER web site (http://peer.berkeley.edu/smcat/search.html) are used as the earthquake loads for calculating the structural earthquake responses.

5.3 Effect of eccentricity

An ideal model of reinforced concrete chimney of 210 meter high is adopted to study the influences of man-made vertical eccentricity in this section. The cross-sectional areas are assumed to be equal in the ideal chimney model with the outer radius of 5.43 meter and the wall thickness of 0.28 meter from the bottom to the top of the reinforced concrete chimney. The bending stiffness EI of the chimney is $2.538\times10^{9}\ \mathrm{kN\cdot m^2}$, shear stiffness GA $3.780\times10^{7}\,\mathrm{kN}$, and axial stiffness EA $1.813\times10^{8}\,\mathrm{kN}$.

Four study cases (see Fig. 7) are adopted here. (1) The equal discrete elements of 10 meters long are used in study case 1 for the ideal chimney. (2) There is a discrete element of 20 meters long between the elevations of 100 and 120 meters in study case 2. The others are also 10 meters long. (3) There are two discrete elements of 20 meters long ranging respectively from 100 to 120 meters and from 40 to 60 meters in the study case 3. The others are also 10 meters long. (4) There are two discrete elements of 20 meters long ranging respectively from 100 to 120 meters and from 160 to 180 meters in the study case 4. The others are also 10 meters long. It can be seen clearly that the man-made vertical eccentricity phenomena arise in the study cases 2, 3 and 4.

Four earthquake records in Table 1 are used as the earthquake loads. The acceleration peaks of the horizontal earthquake records are adjusted to 0.2 g, and the vertical peaks are adjusted to 0.13 g in the following calculations. The small time step of $0.5\,\mathrm{ms}$ is used to decrease the numerical errors of calculations in order to show the influences of vertical eccentricities clearly by considering the eccentricities or not. The damping is neglected.

Study cases 2, 3 and 4 are all used to study the influences of vertical eccentricities by using the man-made unequal discrete elements (see Fig. 7). The time histories of bending moments at the bottom cross section of the ideal chimney are used for comparisons under the actions of four different earthquake waves. In Fig. 8 through Fig. 11, the curves “20 m” correspond to the study case 2, “20 m-20 m (down)” the study case 3 and “20 m-20 m (up)” the study case 4. “Result 10 m”, that is the result obtained from study case 1 (equal spatial-discrete step), is used as the standard solution.

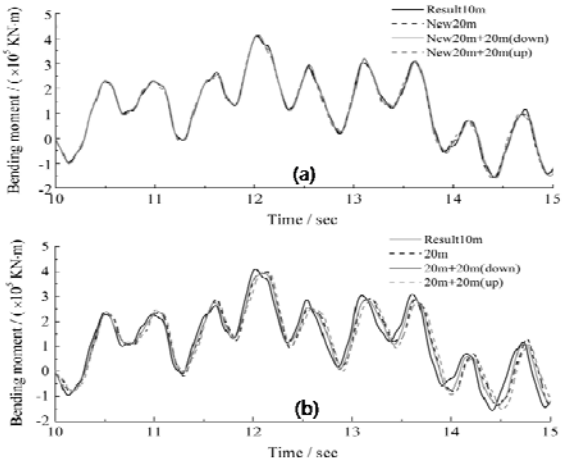

Fig. 8 Time histories of bending moments at the bottom cross section of the ideal chimney under the action of Kocaeli wave: (a) Considering eccentricities and (b) Neglecting eccentricities

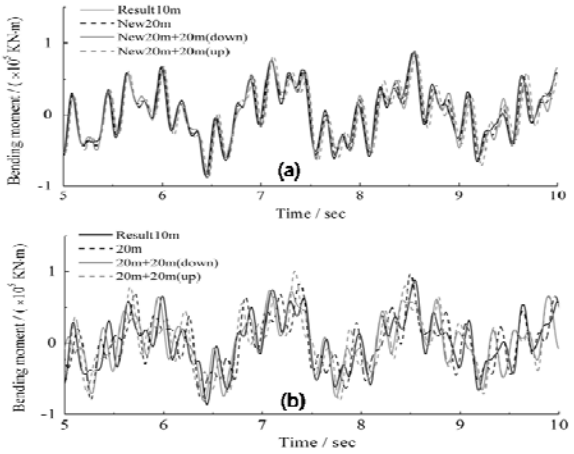

Fig. 9 Time histories of bending moments at the bottom cross section of the ideal chimney under the action of Morgan Hill wave: (a) Considering eccentricities and (b) Neglecting eccentricities

Figs. (a) and (b) in Fig. 8 showed the comparisons of the four study cases considering and neglecting the vertical eccentricities respectively under the action of Cocaeli wave. Fig. 9 is for the Morgan Hill wave, Fig. 10 the Chichi wave and Fig. 11 the Imperial Valley wave.

It can be seen clearly from (a) in Figs. 8 through 11 that the time history curves agree well with the standard solutions (see “Result 10 m” in the Figs) when the eccentricities were considered. Results neglecting the eccentricities (see (b) in Figs. 8 through 11) are not accurate.

It should be pointed that the same conclusions can be obtained for the other time domains in

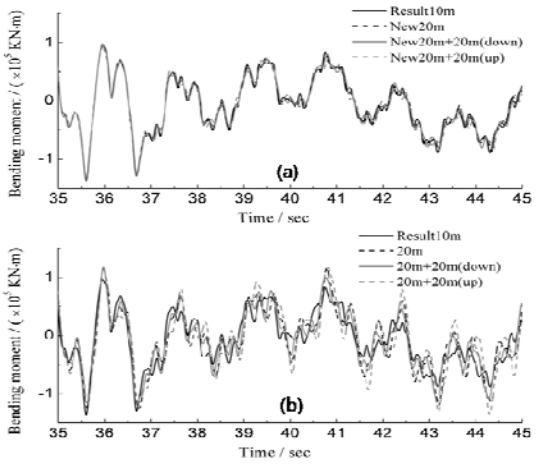

Fig. 10 Time histories of bending moments at the bottom cross section of the ideal chimney under the action of Chichi wave: (a) Considering eccentricities and (b) Neglecting eccentricities

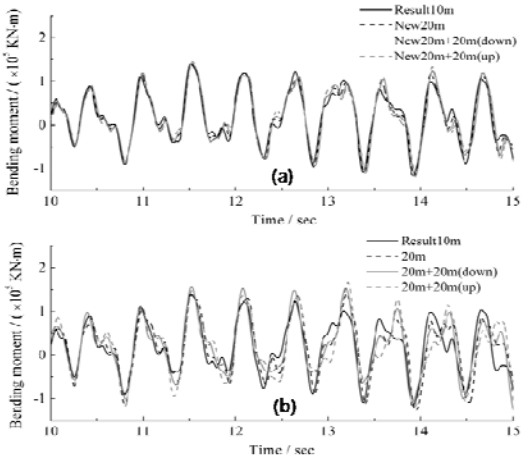

Fig. 11 Time histories of bending moments at the bottom cross section of the ideal chimney under the action of Imperial Valley wave: (a) Considering eccentricities and (b) Neglecting eccentricities

time history. They were omitted in Figs. 8 through 11 in order to show the comparison curves clearly.

The comparing results demonstrate that the method presented in this paper has the correcting function for the vertical eccentricity phenomena in order to provide satisfactory accuracy in the practical evaluations of earthquake response of the tall flexible structure. Namely, it is necessary to consider the vertical eccentricities for the earthquake responses of tall flexible structures when the two adjacent elements posses different cross-sectional areas and different spatial-discrete lengths.

Table 2 Calculation parameters of investigated lumps

Investigated lump	Elevation /m	Mass /10^3 kg	Moment of inertia /kg·m^2	Eccentricity /m	dead load /kN
18	310.1	4	4.04×10^4	-2.75	39.2
17	299.1	12	4.78×10^4	-1.36	156.8
16	286.1	18.7	1.00×10^5	-1.89	340.1
15	270.1	165.13	1.07×10^6	-6.66	1958.3
14	240.4	1081.47	6.04×10^6	0.81	12556.7
13	219.4	359.1	5.92×10^6	0.40	16075.9
12	199.2	1325.79	3.63×10^7	-1.79	29068.7
11	185.8	5678.6	1.41×10^8	-0.15	84718.9
10	171.8	3395.32	2.11×10^8	1.26	117993.1
9	158.8	1322.34	1.45×10^8	-2.19	130952.0
8	137.8	1628.07	1.11×10^8	0.61	146907.1
7	119.8	1624.51	1.21×10^8	-0.09	162827.3
6	101.8	1917.95	1.64×10^8	-1.05	181623.2
5	80.2	2319.79	2.11×10^8	-0.46	204357.2
4	58.6	2820.1	3.30×10^8	-1.48	231994.1
3	32.2	3186.74	3.45×10^8	0.72	263224.2
2	10.1	3992.9	3.22×10^8	0.23	302354.6
1	-10	-	-	-	-

5.4 Earthquake responses of the Nanjing TV transmission tower of 310 meters high

The existing Nanjing TV transmission tower of 310.1 meters high is located in Nanjing city, China. Fig. 12 shows the TV tower. There is a big observation hall at a height of 185.8 meters and a small observation hall at a height of 240.4 meters respectively, connected by a reinforced concrete cylinder tube structure. The part under the big observation hall consists of three prestressed concrete legs with hollow rectangular sections. Over the small observation hall there is also a reinforced concrete square tube structure between the height of 246.61 meters and 270.1 meters. There are three hollow square steel tubes of different cross-sectional areas above the elevation of 270.1 meters.

In the practical calculation, the structure of the three prestressed concrete legs is described by using such a model that consists of some cylinder-shaped tubes with their cross-sectional areas and moments of inertia of the cross-sectional area equivalent to the corresponding quantities of the original structure provided in the Table 2 in Wu and Li's literature (Wu 2004).

The parameters in the Table 2 in Wu and Li's literature are used here and the other parameters used for studying the Nanjing TV tower are shown in Table 2 in this paper, which are calculated based on the data in Wu and Li's Table 2 that has been obtained from the design drawings of the TV tower.

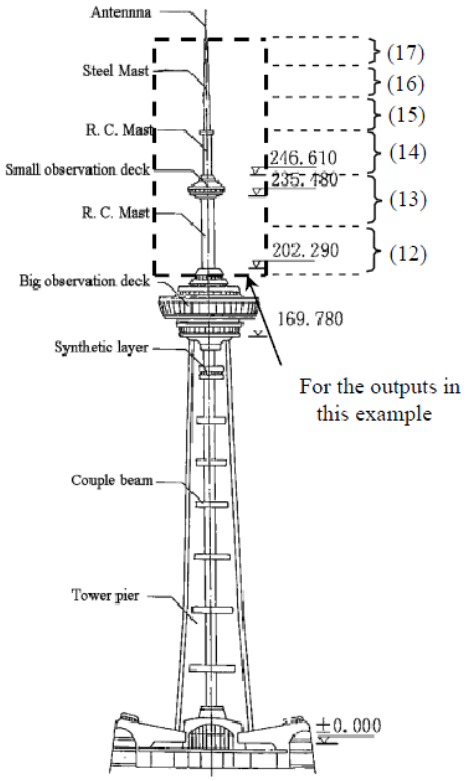

Fig. 12 The Nanjing TV Tower (Wu and Li 2004)

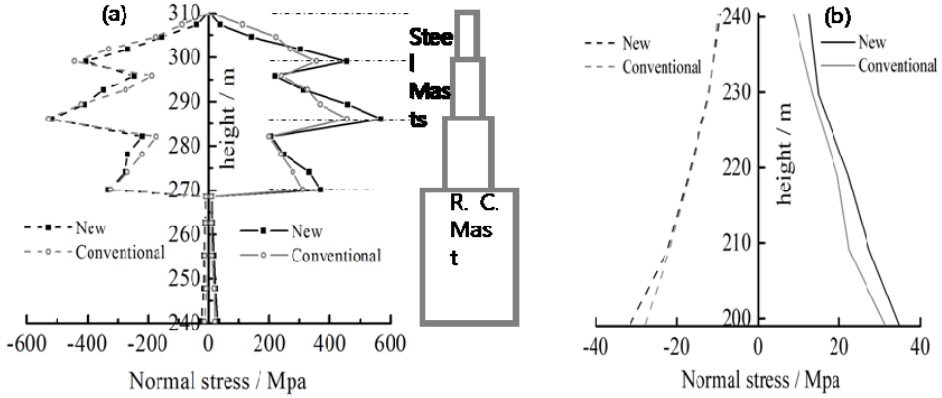

Fig. 13 Spatial distributions of maximum normal stresses at different cross sections of the TV tower under the action of Kocaeli wave: (a) for the masts above the small observation hall and (b) for the mast between the small and the big observation halls. Solid and dash lines denote the compressive and tensile stresses respectively

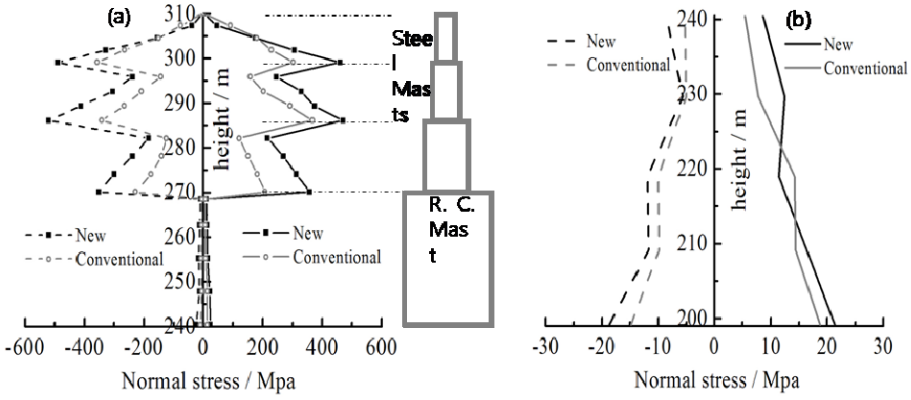

Fig. 14 Spatial distributions of maximum normal stresses at different cross sections of the TV tower under the action of Morgan Hill wave: (a) for the masts above the small observation hall and (b) for the mast between the small and the big observation halls. Solid and dash lines denote the compressive and tensile stresses respectively

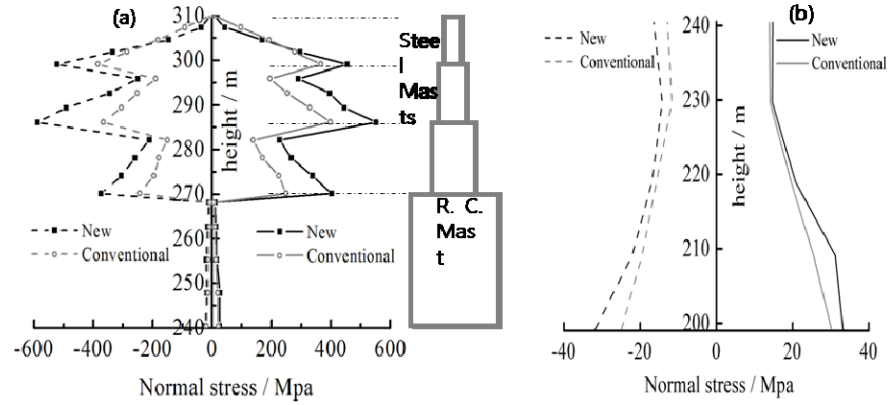

Fig. 15 Spatial distributions of maximum normal stresses at different cross sections of the TV tower under the action of Chichi wave: (a) for the masts above the small observation hall and (b) for the mast between the small and the big observation halls. Solid and dash lines denote the compressive and tensile stresses respectively

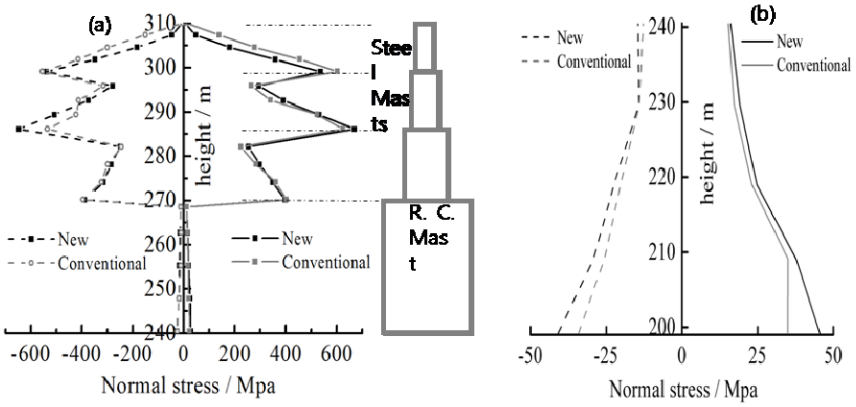

Fig. 16 Spatial distributions of maximum normal stresses at different cross sections of the TV tower under the action of Imperial Valley: (a) for the masts above the small observation hall and (b) for the mast between the small and the big observation halls. Solid and dash lines denote the compressive and tensile stresses respectively

Four earthquake records in Table 1 are also used here to analyze the earthquake responses of the Nanjing TV communication tower. The time step is 1.0 ms . The damping is also neglected.

In Figs. 13 through 16, “New” denotes the results given by the method presented in this paper, and “Conventional” denotes the conventional results with both vertical eccentricity and rotary inertia neglected. Solid lines denote the compressive stresses and dash lines the tensile stresses. Figs. (a) and (b) show respectively the spatial distributions of peak normal stresses of the mast above the small observation hall and the mast between the small and the big observation halls.

Fig. 13 is for the earthquake load of Kocaeli wave, Fig. 14 the Morgan Hill wave, Fig. 15 the Chichi wave and Fig. 16 the Imperial Valley wave.

The horizontal and vertical acceleration records are used as the input data for getting the earthquake response of the Nanjing TV tower. The mass and the moment of inertia of the foundation are not required because the fixed-base model was adopted. Therefore they are not calculated in Table 2 (see investigated lump 1).

From figure (a) in Figs. 13 through 16, it can be seen that the tensile stresses and compressive stresses reach their biggest values at the root of second steel mast at the elevation of 286.1 meters. The curves of tensile stress and compressive stress were zigzag shapes because there are three steel masts of different cross-sectional areas. The small amount of data used to plot the figure also causes the curves to be zigzag shapes.

It can be seen that the peak value of normal stress at the root of second steel mast increases when the existing vertical eccentricity phenomenon is considered. The peak value of compressive stress increases by 25% for the Kocaeli wave. The peak compressive and tensile stresses increase by 28% and 52% respectively for the Morgan Hill wave, 39% and 63% respectively for the Chichi wave and 7% and 21% respectively for the Imperial Valley wave.

It can be seen from Fig. (b) in Figs. 13 through 16 that the bottom stresses of reinforced concrete mast, that connects the small and the big observation halls, increase also when the vertical eccentricity phenomenon is considered. The bottom tensile stress increases by 13% for the Kocaeli wave, 26% for the Morgan Hill wave, 28% for the Chichi wave and 20% for the Imperial Valley wave.

The results obtained above demonstrated that the conventional calculating results of stresses might be lower than their real values of earthquake response. The steel mast of the TV tower might tend to dangerous if some special earthquakes occur.

It has been reported that the wind-induced acceleration response of the small observation hall under strong winds was too high to meet the comfort requirement (Wu 2004). In this study it is found that peak acceleration of the small observation hall increases by 7.1% for the Kocaeli wave, 29.2% for the Morgan Hill wave and 26.5% for the Chichi wave, but decreases by 13.4% for the Imperial Valley wave when the vertical eccentricity phenomenon is considered.

It is expected that the cognitions in this investigation are interesting and useful to researchers and designers involved in designing TV towers.

6. Conclusions

A method was presented for the earthquake response analyses of tall flexible structures based on beam models. The method is available in dealing with the existing vertical eccentricity phenomenon between the spatial-discrete nodes and the corresponding centroids of investigated lumps. The extra moments caused by the vertical dead loads and axial forces from vertical deformations are considered in the study. The modified dynamic equilibrium equations were derived for the stick MDOF model of tall flexible structure based on beam theory. It shows that the modified mass matrix and assemblage of stiffness matrix should be used instead of the conventional mass matrix and assemblage of stiffness matrix that are commonly used in the stick MDOF model. The numerical results demonstrate that it is necessary to consider the vertical eccentricities in order to obtain the accurate earthquake response for designing the tall flexible structure to avoid danger. The earthquake responses of Nanjing TV tower were studied under the actions of four earthquake waves in Rock, Soft rock, Stiff soil and Soft soil respectively. The numerical results demonstrate that the peak stress values of the masts of Nanjing TV tower obtained by using the conventional dynamic equations are lower than the evaluations given by the method presented in this paper, especially for the steel masts above the small observation hall. The cognitions obtained in this paper are expected to be useful for the researchers and designers to design the tall flexible structures such as tall TV transmission towers and tall reinforced concrete chimneys. The method presented here can be extended to the evaluations of inelastic response of tall flexible structures by using the incremental form of the modified dynamic equilibrium equations if the corresponding hysteretic behaviors are known.

Acknowledgments

The authors thank the National Natural Science Foundation of China for the support of this study (grant no. 10972144).

References

Akinci, N.O. (2009), "An investigation on seismic resistance of reinforced concrete industrial chimneys", *Proceedings of the 2009 Structures Congress - Don't Mess with Structural Engineers: Expanding Our Role*, 964-971.

Cao, H., Reinhorn, A.M. and Soong, T.T. (1998), "Design of an active mass damper for a tall TV tower in Nanjing, China", *Eng. Struct.*, **20**(3), 134-143.

Feng, M.Q., Kim, J.M. and Xue, H. (1998), "Identification of a dynamic system using ambient vibration measurements", *J. Appl. Mech. Trans. ASME*, **65**(4), 1010-1021.

Feng, Maria Q. and Zhang, R. (1997), "Wind-induced vibration characteristics of Nanjing TV tower", *Int. J. Nonlinear Mech.*, **32**(4), 693-706.

Gould, P.L. and Huang, W. (2006), "Higher mode effects in the nonlinear static analysis of a collapsed chimney", *Proceedings of the 2006 Structures Congress and Exposition*, 19.

Gould, P.L. and Huang, W. (2009), "Nonlinear analysis of a collapsed reinforced concrete chimney", *Proceedings of the 2009 Structures Congress - Don't Mess with Structural Engineers: Expanding Our Role*, 994-999.

Goyal, A. and Maiti, M.K. (1997), "Inelastic seismic resistance of reinforced concrete stack-like structures", *Earthq. Eng. Struct. D.*, **26**(5), 501-513.

Huang, W. and Gould, P.L. (2007), "3-D pushover analysis of a collapsed reinforced concrete chimney", *Finite Elem. Anal. Des.*, **43**(11-12), 879-887.

Huang, W., Gould, P.L., Martinez, R. and Johnson, G.S. (2004), "Non-linear analysis of a collapsed reinforced concrete chimney", *Earthq. Eng. Struct. D.*, **33**(4), 485-498.

Halabian, A.M., Elnaggar, M.H. and Vickery, B.J. (2002), "Nonlinear seismic response of reinforced-concrete free-standing towers with application to TV towers on flexible foundations", *Struct. Des. Tall Build*, **11**(1), 51-72.

Khaloo, A.R., Asadpour, N. and Horr, A.M. (2001), "Full dynamic analysis of Tehran telecommunication tower; linear and nonlinear responses", *Struct. Des. Tall Spec. Build.*, **10**(4), 263-281.

Kolsky, H. (1953), *Stress wave in solids*, Oxford, Clarendon Press, 71.

Reinhorn, A.M., Soong, T.T. and Cao, H. (1995), "Preliminary evaluation of wind induced response of Nanjing TV tower", *Report of US/PRC Coordination Program,* State University of New York at Buffalo, Buffalo, NY.

Wu, J.R. and Li, Q.S. (2004), "Finite element model updating for a high-rise structure based on ambient vibration measurements", *Eng. Struct.*, **26**(7), 979-990.

Wu, J.C. and Yang, J.N. (2000), "LQG control of lateral-torsional motion of Nanjing TV transmission tower", *Earthq. Eng. Struct. D.*, **29**(8), 1111-1130.

Wilson, J.L. (2003), "Earthquake response of tall reinforced concrete chimneys", *Eng. Struct.*, **25**(1), 11-24.

Yahyai, M., Rezayibana, B. and Daryan, A.S. (2009), "Nonlinear seismic response of milad tower using finite element model", *Struct. Des. Tall Spec. Build.*, **18**, 877-890.

CC

Appendix A

Matrices K_u, $K_{u\theta}$, $K_{\theta u}$, K_θ, K_θ^I and $K_{\theta u}^I$ are respectively the assemblies of K_u^j, $K_{u\theta}^j$, $K_{\theta u}^j$, K_θ^j, K_θ^{Ij} and $K_{\theta u}^{Ij}$ where

$$K_u^j = \begin{bmatrix} K_1^j & -K_1^j \\ -K_1^j & K_1^j \end{bmatrix}, \quad K_{u\theta}^j = \begin{bmatrix} -K_2^j & -K_2^j \\ K_2^j & K_2^j \end{bmatrix}, \quad K_{\theta u}^j = \begin{bmatrix} K_1^j \frac{h_j}{2} + \frac{N_j}{2} & -K_1^j \frac{h_j}{2} - \frac{N_j}{2} \\ K_1^j \frac{h_j}{2} + \frac{N_j}{2} & -K_1^j \frac{h_j}{2} - \frac{N_j}{2} \end{bmatrix},$$

$$K_{\theta u}^{Ij} = \begin{bmatrix} -z_{ci}K_1^j & z_{ci}K_1^j \\ z_{ci+1}K_1^j & -z_{ci+1}K_1^j \end{bmatrix}, \quad \left[K_\theta^j\right] = \begin{bmatrix} (K_5^j - \frac{N_j h_j}{8}) - K_2^j \frac{h_j}{2} & -(K_5^j - \frac{N_j h_j}{8}) - K_2^j \frac{h_j}{2} \\ -(K_5^j - \frac{N_j h_j}{8}) - K_2^j \frac{h_j}{2} & (K_5^j - \frac{N_j h_j}{8}) - K_2^j \frac{h_j}{2} \end{bmatrix},$$

$$K_\theta^{Ij} = \begin{bmatrix} z_{ci}K_2^j & z_{ci}K_2^j \\ -z_{ci+1}K_2^j & -z_{ci+1}K_2^j \end{bmatrix}.$$

As for matrix $K_{\theta u}^{/}$, the element $k_{ii}^{/}$ in it should be assembled respectively for $z_{ci} > 0$ and $z_{ci} < 0$ cases. Noting the case $z_{cn} > 0$ does not exit for the top investigated lump and the $z_{c1} < 0$ case does not exit for the bottom investigated lump, the matrix $K_{\theta u}^{/}$ is written in the following form

$$\left[K_{\theta u}^{/}\right] = \begin{bmatrix} a_1 N_1 & -a_1 N_1 & 0 & & & & \\ & & \ddots & & & & \\ & & k_{i\,i-1}^{/} & k_{i\,i}^{/} & k_{i\,i+1}^{/} & & \\ & & & & \ddots & & \\ & & & & 0 & -(a_n^{/}+1)N_{n-1} & (a_n^{/}+1)N_{n-1} \end{bmatrix}.$$

It should be noted that the element $k_{ii}^{/}$ in $K_{\theta u}^{/}$ for $z_{ci} > 0$ case is different from that for the $z_{ci} < 0$ cases. If $z_{ci} > 0$, then $k_{i\,i-1}^{/} = 0$, $k_{i\,i}^{/} = a_i(-N_{j-1} + N_j)$, and $k_{i\,i+1}^{/} = -k_{i\,i}^{/}$. If $z_{ci} < 0$, then $k_{i\,i-1}^{/} = -k_{i\,i}^{/}$, $k_{i\,i}^{/} = (a_i^{/}+1)(N_{j-1} - N_j)$, and $k_{i\,i+1}^{/} = 0$. Variable z_{ci} is involved in a_i and $a_i^{/}$. The other elements in matrix $K_{\theta u}^{/}$ vanish. When $z_{ci} = 0 \quad (i = 1, 2, \cdots, n)$, matrix $K_{\theta u}^{/}$ vanish.

As for matrix $K_\theta^{/}$, the element $k_{ii}^{/}$ in it should also be assembled respectively for $z_{ci} > 0$ and $z_{ci} < 0$ cases. Matrix $K_\theta^{/}$ is written as follows

$$\left[K_\theta^{/}\right]=\begin{bmatrix} (b_1-\frac{z_{c1}^2}{2h_1}+z_{c1})N_1 & (b_1+\frac{z_{c1}^2}{2h_1})N_1 & 0 & & \\ & \ddots & & & \\ & k_{i\,i-1}^{/} & k_{i\,i}^{/} & k_{i\,i+1}^{/} & \\ & & \ddots & & \\ 0 & [-b_n^{/}+\frac{(h_{n-1}+z_{cn})^2}{2h_{n-1}}-(h_{n-1}+z_{cn})]N_{n-1} & [-b_n^{/}-\frac{(h_{n-1}+z_{cn})^2}{2h_{n-1}}]N_{n-1} & & \end{bmatrix}$$

The element $k_{ii}^{/}$ in $K_{\theta u}^{/}$ for $z_{ci}>0$ case is also different from that for the $z_{ci}<0$ cases. If $z_{ci}>0$, $k_{i\,i-1}^{/}=0$, $k_{i\,i}^{/}=(b_i-\frac{z_{ci}^2}{2h_j}+z_{ci})(-N_{j-1}+N_j)$, and $k_{i\,i+1}^{/}=(b_i+\frac{z_{ci}^2}{2h_j})(-N_{j-1}+N_j)$. If $z_{ci}<0$, $k_{i\,i-1}^{/}=[b_i^{/}-\frac{(h_{j-1}+z_{ci})^2}{2h_{j-1}}+(h_{j-1}+z_{ci})](-N_{j-1}+N_j)$, $k_{i\,i}^{/}=[b_i^{/}+\frac{(h_{j-1}+z_{ci})^2}{2h_{j-1}}](-N_{j-1}+N_j)$, and $k_{i\,i+1}^{/}=0$. The other elements in matrix $K_\theta^{/}$ vanish. When $z_{ci}=0$ $(i=1,2,\cdots,n)$, matrix $K_{\theta u}^{/}$ vanish.